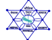

(ANPA Conference 2023)
ISSN: 2392-473X(Print), 2738-9537 (Online)

Review Article ©Nepal Physical Society
DOI: http://doi.org/10.3126/jnphyssoc.v9i3.62454

Al-rich AlGaN Alloys: Unique Materials for Deep UV LEDs

Mim Lal Nakarmi[a)]

Department of Physics, Brooklyn College and the Graduate Center of the City University of New York, Brooklyn, NY 11210, USA.

[a)]*Electronic mail: mlnakarmi@brooklyn.cuny.edu*

Abstract. Energy bandgap of $Al_xGa_{1-x}N$ alloys can be tuned systematically from ~ 3.4 to 6.1 eV by changing the alloy composition (x) from 0 to 1 and the direct bandgap nature is maintained in the entire range of alloy compositions which make the AlGaN alloys suitable materials for the development of light emitting diodes (LEDs) covering the ultraviolet (UV) spectral region from 210 to 400 nm. For LEDs in the deep UV regions ($\lambda < 300$ nm), Al-rich AlGaN alloys of Al content higher than 50% are required. Deep UV LEDs have applications in a wide range of fields including display, disinfection, medical, sensing, and communication. With recent progress in the material growth and electrical conductivity, Al-rich AlGaN alloys have emerged as unique wideband gap materials for the development of deep UV LEDs. In this review article, how the progress of Al-rich AlGaN alloys has made in terms of the material growth and electrical conductivity leading its emergence as deep UV materials have been reviewed. Challenges and prospects of the deep UV LEDs to improve the performance of the devices will also be discussed.

Received: 1 August, 2023; **Revised**: 15 November, 2023; **Accepted**: 22 December, 2023

Keywords: Al-rich AlGaN alloys, deep UV, Light emitting diodes, conductivities

INTRODUCTION

Energy bandgap of III-nitride compounds- indium nitride (InN), gallium nitride (GaN), aluminum nitride (AlN), and their alloys ranges from 0.7 to 6.1 eV which makes them promising materials for optical applications such as photo detectors and emitters covering the spectral range from infrared to deep ultraviolet (UV) region [1–4]. GaN with bandgap of 3.42 eV is the central binary compound of III-nitride family and has success stories in the development of blue light emitting diode (LED) and electronic devices. The success of GaN based blue LEDs was made possible mainly due to the two major breakthroughs in the GaN material technology- use of a low temperature buffer layer in the growth of GaN epilayer on foreign substrates, and achievement of p-type conductivity by magnesium (Mg) doping and subsequent annealing [5–10]. Significant progress has been made after the demonstration of efficient blue LEDs in 90s and blue LEDs with external efficiency of more than 80% has been achieved [11]. GaN-based LEDs and laser diodes (LDs) are now being produced on an industrial scale changing the areas of illumination. Nowadays, these products can be found in our daily life in household displays, street lamps, TV, cars, Blue-ray players, etc.

The wavelength (or energy of photon) of the optical emission from LEDs depends on the bandgap of the material used in the active region. Blue emission is produced by making an active region of InGaN multiple quantum wells (MQWs) with GaN barriers. The active region is sandwiched between n-type GaN and p-type GaN in the LED structure. When external bias is applied to the diode structure, electrons from n-type region and holes from p-type region are injected into the active region and optical emission is produced by the recombination of electrons and holes confined in the quantum wells (QWs). In order to tune the wavelength of the optical emission, the bandgap of the materials used in the active region should be increased (decreased) for shorter (longer) wavelength and it should maintain the direct bandgap nature. After the success of blue LEDs, efforts of developing nitride-based LEDs began in both directions, shorter and longer wavelengths. In the early 21st century, there was a great effort of developing LEDs in deep UV region driven by DARPA's Semiconductor Ultraviolet Optical Sources (SUVOS) program for application in portable biochemical agent detection as absorption peak for Tryptophan, a common constituent of biological organisms is at 280 nm [12]. Materials with bandgap higher than GaN are required to produce emissions in the deep UV region. Bandgap of GaN can be increased by alloying with AlN. Bandgap of $Al_xGa_{1-x}N$ alloys can be increased system-

atically by changing the alloy composition (x) from 0 to 1 and the direct bandgap nature is maintained throughout the alloy range. Thus, AlGaN alloys are obvious choice of material for the development of deep UV LEDs. Significant progress in the development of LEDs in deep UV regions has been made in the last two decades, especially at wavelength around 280 nm with output powers in the order of milliwatt [13–16]. Deep UV LEDs of wavelengths shorter than 280 nm were also reported [17–21]. The shortest wavelength reported so far is AlN-based LED at 210 nm [22].

Deep UV LEDs can replace mercury-based fluorescent lamps for general-purpose lighting system. Fluorescent lamps use atomic emissions from mercury vapor peaks at 184.5 and 253.7 nm to convert into white light using phosphor. LED-based general purpose lighting systems will be efficient, cheaper, and tunable for color temperature. After the Covid-19 pandemic, there has been a big demand for portable light sources in the deep UV region for disinfection since they are germicidal radiations. Commercial products of appliances for the uses in the buildings are being redesigned for the purpose of air purification, water purification, disinfection, and surface decontamination using the deep UV LEDs. Since LEDs are solid-state and small-size devices, they are easy to employ. High demand for deep UV LEDs on an industrial scale has made another surge in the research and development in recent years to improve the material quality and performance of the deep UV LEDs.

There are several other expanding applications of deep UV light in UV curing in industry, sterilization, diagnosis and treatment in the medical field, wastewater treatment, gas sensing, non-line of sight (NLOS) communication, and many others [23]. It should also be aware that exposure to deep UV light can have severe effects on animals and human beings. For example, deep UV light in UVB region (280 – 320 nm) can cause terrible sunburn on skin, and UVC (100 – 280 nm) can damage DNA structure.

There were also efforts to develop oxide-based wide bandgap materials such as zinc oxide, magnesium oxide and their alloys as alternate to the nitrides. However, achieving stable p-type conductivity is the biggest hurdle developing the oxide based optical emitters [24]. Thus, Al-rich AlGaN alloys have become unique materials for the deep UV LEDs application. In this article, how the development of Al-rich AlGaN alloys has progressed as deep UV materials and recent progress in the material growth and conductivity of Al-rich AlGaN alloys will be reviewed. Fundamental aspects of these materials are better known today but there are still several issues and technical challenges for improving the performance of the Al-rich AlGaN alloys-based deep UV LEDs in terms of material quality, n-and p-type conductivity, device structure design and device fabrication. Prospects of material development and deep UV LEDs will also be discussed.

AlN as reference point for the growth of Al-rich AlGaN alloys

In the early stage of developing deep UV LEDs, efforts were made to use GaN as the reference point for the growth of material since it was well known in terms of material technology and fundamental properties. So, AlGaN alloys were grown by alloying GaN with AlN to increase the bandgap. However, increasing Al content in the AlGaN alloys also adds complexity in terms of crystalline quality, conductivity, and optical quantum efficiency. Growth of alloys is different from binary compounds. As-grown GaN epilayers are normally n-type. With increasing Al content in the AlGaN alloys, the conductivity of undoped AlGaN alloys decreases sharply and often becomes an insulator for $x > 0.4$ [25]. Even with Si doping in AlGaN alloys, conductivity decreases with increasing Al content mainly due to the deepening of Si donor level and compensation with acceptor like defects [26]. The issue was even severe in the case of magnesium doping for p-type conductivity. Currently, it is well known that high crystalline quality of the material is important to control the conductivity of AlGaN alloys and enhance the quantum efficiency [27].

For LEDs with emission in the deep UV wavelengths < 300 nm, Al-rich AlGaN alloys with Al content higher than 50% are required. Since this region is far from the GaN, the issues of material growth for higher Al content, as mentioned above, were difficult to resolve when GaN was used as the reference point. So, the strategy of using AlN as the reference point was made for the growth of Al-rich AlGaN alloys. AlN is the high-end binary point in the nitride system and has bandgap of ~ 6.1 eV [4]. In order to understand the nature of AlGaN in the whole alloy range, it is also important to gain knowledge of AlN. Developing methods to grow high-quality AlN was needed to use the AlN as a reference point. Once high-quality AlN was achieved, the next strategy was to grow Al-rich AlGaN epilayers on AlN and change the alloy composition by alloying with GaN.

Growth of Aluminum Nitride on sapphire

Nitrides are normally grown on the foreign substrates such as sapphire or silicon carbide. Sapphire is widely used as it is cost effective, and it is also transparent to the deep UV light. The wurtzite crystal structure of AlN has $\sim 13\%$ lattice mismatch with sapphire in (0001) direction. In 1983, it was discovered that the insertion of a low temperature buffer layer of AlN before the growth of epilayer improves the crystalline quality of GaN significantly [5–7]. Later, it was found that employing a low-temperature buffer layer of GaN can further improve the crystalline quality of GaN epilayers [10]. A typical growth tempera-

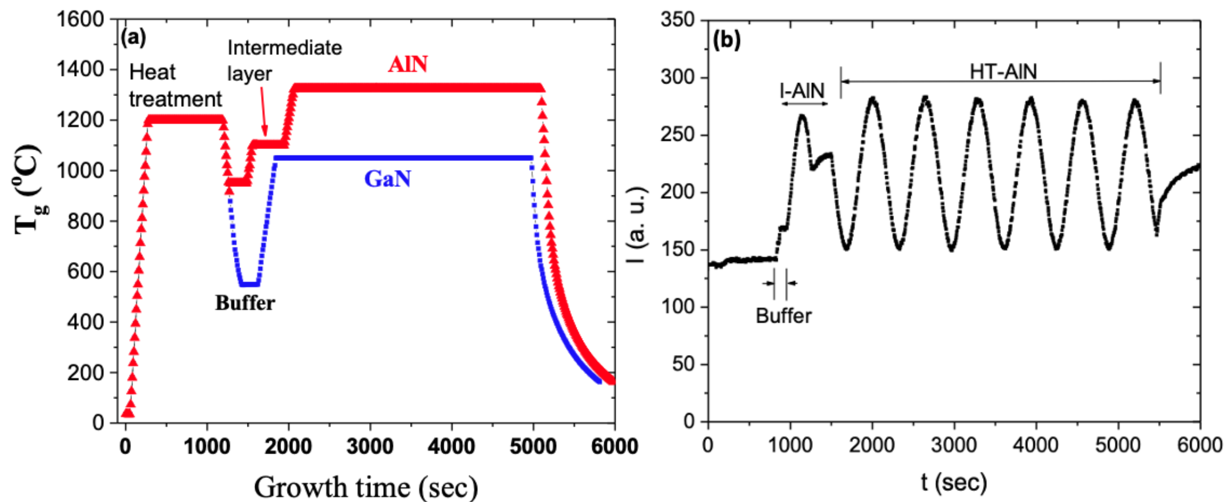

FIGURE 1. a. Growth temperature profile of GaN and AlN epilayers, b. Reflection interference pattern during the growth of AlN in MOCVD. Inset is the schematic diagram of layer structure in three-step growth method of AlN on sapphire substrate. [Ref 29]

ture profile for the growth of GaN in this two-step method by metal organic chemical vapor deposition (MOCVD) technique is shown in Fig.1a. Heat treatment of sapphire is done around 1200 °C before starting the growth of materials. The vapor of metal organic precursors, trimethyl gallium and trimethyl aluminum are used as the sources of gallium and aluminum, respectively. Ammonia gas is used as the source of nitrogen. A thin buffer layer is first grown at low temperature around 550 °C followed by high temperature growth of GaN epilayer at temperature around 1050 °C in the reactor pressure of 300 torr.

Similar to the growth of GaN, insertion of buffer is required to grow AlN on the sapphire substrates. The growth of AlN has additional problems due to the low surface migration of Al adatoms and parasitic gas reaction between aluminum source and ammonia [28]. High growth temperature and low pressure are thus required for the growth of AlN to provide enough mobility to aluminum adatoms. It is now well known that the growth temperature of higher than 1300 °C and low pressure are required to grow the high quality AlN epilyer using MOCVD technique. Various methods were developed to improve the material quality of AlN, for example, three-step growth, pulsed growth, use of alternating V/III ratio, nitridation of the substrate, multilayers with pulse ammonia, hydride vapor phase epitaxy (HVPE) and epitaxial lateral overgrowth [17, 29–35]. Clearly, the growth conditions and growth mechanism of AlN on sapphire are different from that of GaN on sapphire. As the growth temperature of AlN is higher than that of GaN, optimization of buffer layer is crucial for the high crystalline quality of AlN on sapphire. We developed a three-step growth method by modifying the buffer layer using MOCVD technique [29]. The growth temperature profile of this method is also shown in Fig. 1a. In this three-step method, a thin low temperature buffer is first grown at 950 °C and an intermediate layer of thickness ∼120 nm is grown at 1100 °C, followed by a thick epilayer of AlN grown at high temperature ∼1325 °C. The growth pressure is 50 torr. The schematic layer diagram for this method is also shown in the inset of Fig. 1b. This method can produce AlN epilayer of high optical quality with room temperature PL emission intensity of band-edge comparable to that of GaN and low density of screw dislocations [36, 37]. The full width at half maximum (FWHM) of XRD rocking curves of the (0002) and (1012) reflection planes were 63 and 437 arcsec, respectively for AlN epilayer [37]. Estimated density of threading dislocations from both XRD and TEM are ∼ 2.5 x 10^9 cm^{-2} for edge type and ∼ 5 x 10^6 cm^{-2} for screw type dislocations. Screw type dislocation density of AlN epilayers produced by this method is very low but dominating dislocations are edge type.

Figure 1b shows a typical in-situ reflection interference pattern during the growth of AlN epilayer on sapphire using the three-step growth method. Based on the in-situ reflection interference pattern during the growth of AlN, the early-stage growth is different from that of GaN. In the case of GaN, after the deposition of low temperature buffer layer, intensity of the interference pattern decreases while ramping up the growth temperature and in the initial stage of the high temperature growth [38, 39]. The thin buffer layer first forms clusters of coalesced nucleation layer making surface rough. Lateral growth dominates in the beginning of the high temperature growth of GaN until all coalesced clusters are leveled and reflectivity starts increasing. This early stage of growth during which reflectivity decreases plays an important role in re-

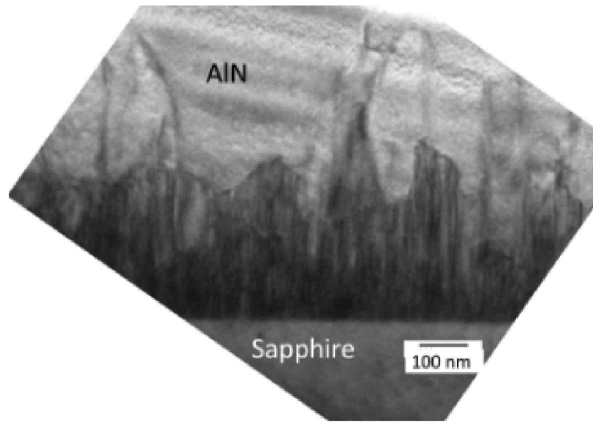

FIGURE 2. Cross-section TEM image of AlN epilayer grown by three-step method using MOCVD.

ducing the threading dislocation density of GaN. In the case of AlN, we found that decrease of reflectivity was not observed after low temperature buffer. If the intensity is dropped, it is very difficult to recover the reflectance signal which ultimately leads to a rough surface. Insertion of the intermediate layer in the three-step growth was critical in reducing the dislocation density of AlN.

Based on the transmission electron microscopy (TEM) analysis of the AlN epilayer grown on sapphire substrates by the three-step method, it is revealed that the insertion of the intermediate layer helps reduce the density of threading dislocations. Figure 2 shows a cross section TEM image of an AlN epilayer grown by the three-step method. Generation of threading dislocations can be clearly seen at the interface of sapphire and AlN. Most of the threading dislocations are annihilated within the thickness of $\sim$300 nm and AlN epilayer with very low dislocation grows onward. It is believed that the insertion of the intermediate layer helps bending the threading dislocations and ultimately the threading dislocations are annihilated. The threading dislocation densities estimated from the TEM images are consistent with the XRD analysis.

Using the AlN grown on sapphire by this method, photodetectors with cut-off wavelength of 200 nm were demonstrated [40]. The availability of high quality AlN also made it possible to gain knowledge on the fundamental properties such as precise band structure and bandgap of the material, and the nature of excitons [4]. The order of the valance bands in AlN is different from that of GaN. The Γ_7 is the topmost valence band in AlN whereas it is Γ_9 in GaN resulting the dominant PL emission of GaN is with polarization of $E \perp c$ while the dominant emission of AlN is with polarization of $E \parallel c$. Cross over of the valence bands in $Al_xGa_{1-x}N$ alloy occurs around $x \sim 0.25$ [41]. Consequence of this fundamental property leads to the difficulty in light extraction in Al-rich AlGaN based LEDs and the LDs with $Al_xGa_{1-x}N$ as active layers ($x > 0.25$) will have dominant laser emission in the TM mode.

Among other growth techniques of AlN epilayers grown on sapphire, pulse-flow of ammonia with multilayer growth technique is impressive to lower the edge-type dislocation by one order. The edge- and screw-type dislocation densities are 7.5×10^8 cm^{-2} and 3.8×10^7 cm^{-2}, respectively for the AlN layers grown on sapphire by this method [17]. For further reduction of threading dislocation density, advanced growth technique such as epitaxial lateral overgrowth has been investigated [35]. The dislocation density of the AlN layer grown by this method is less than 10^7 cm^{-2}. Impressive progress in the growth of bulk single-crystal AlN substrate has been made in the last two decades. Wafer size (2 inch) AlN single crystal substrates are available commercially [42–44]. Average dislocation density of AlN single crystal substrates is around 10^3 cm^{-2}. Materials with low dislocation density are required to enhance the internal quantum efficiency. Growth of AlN epilayer and device structure on the native substrate is ideal as the problem due to the lattice and thermal mismatches can be avoided. AlN epilayer with significantly reduced dislocation density can be expected when grown on AlN native substrate.

N- type conductivity of Al-rich AlGaN alloys

Achieving both n- and p-type conductivities are essential for realizing bipolar devices such as LEDs. Electrical conductivity of semiconductors depends on the concentration and mobility of the carriers. As-grown GaN epilayers are normally n-type. It is believed that the source of the donor in GaN is unintentionally doped oxygen, whose activation energy is about 30 meV [45–47]. With increasing Al content in the AlGaN alloys, the activation energy of the donor also increases. Thus, the conductivity of undoped $Al_xGa_{1-x}N$ alloys decreases and often becomes an insulator for $x > 0.4$ [25]. It was proposed that the decrease of conductivity with increasing Al content in undoped $Al_xGa_{1-x}N$ is due to the transition of oxygen from shallow donor into a deep donor, so called DX center [48]. Silicon (Si) is a shallow donor with activation energy $\sim$ 30 meV in GaN which is widely used as an intentional dopant to control the n-type conductivity of nitrides [49]. With increasing Al content of AlGaN alloys, activation energy of Si donor also increases. Activation energy of Si in AlN is estimated to be 85-180 meV [27, 50]. Thus, the concentration of electrons decreases with increasing Al content in AlGaN alloys even with Si doping due to the deepening of Si donor level. Theoretical calculations and some experimental evidence also predicted that Si could become DX center in AlGaN alloys for Al content higher than 50% [51, 52]. Another reason of decreasing conduc-

tivity is due to the compensation by acceptor like defects [26]. Based on the first principles calculations, formation energies of the compensating defects such as cation vacancies with triple negative charges, and cation vacancy complexes with double and single charge states, are low in Al-rich AlGaN alloys and AlN. Extrapolation of conductivities from the low Al content AlGaN alloys also indicated that achieving conductive Al-rich AlGaN alloys could be impossible.

Three major issues needed to be resolved to improve the n-type conductivity of Al-rich AlGaN alloys: increased threading dislocation density and deepening of Si donor level with increasing Al content, and electrical compensation by acceptor like defects. The issue of producing high quality AlGaN alloys with low density of dislocations was first addressed. Consequently it provided a path to tackle the remaining issues of high activation energy of dopants, controlling compensating defects, and solubility of dopants. The success of producing high quality AlN epilayers made a basis for the growth of high quality Al-rich AlGaN epilayer by using the AlN as template. In this scheme, AlN epilayer is first grown on sapphire and then Al-rich AlGaN alloy is grown subsequently on the AlN as template. The dislocation density of Al-rich AlGaN alloys was dramatically reduced with this scheme. It is now routine practice that all Al-rich AlGaN alloys-based devices are grown on AlN templates.

After the success of growing high crystalline quality Al-rich AlGaN alloys on high quality AlN templates, strategy used to enhance the conductivity was by employing heavy silicon doping to increase the concentration of electrons and controlling compensating defects. Number of free carriers contributed by the dopant is negative exponential function of activation energy (E_A) as given below,

$$n = N_d exp^{-\left(\frac{E_A}{k_B T}\right)}, \tag{1}$$

where, n is the concentration of the carrier (electron or hole), N_d, k_B, and T are dopant concentration, Boltzmann constant, and absolute temperature, respectively. As the concentration of carriers will be low for large E_A, increasing N_d by heavy doping can enhance the electron concentration in the AlGaN alloys. Heavy doping by Si was successful in achieving n-type conductivity in the Al-rich AlGaN alloys. Heavy Si doping might form an impurity band and bandgap renormalization can occur due to the screening effect which could lower the effective activation energy of Si donors. Heavy doping, however, could decrease the mobility due to impurity scattering.

Theoretical results from the first principles calculations were very useful for addressing the issue of compensation by point defects. Cation vacancies and their complexes have lowest formation energy in n-type condition, i.e., when Fermi level is near the conduction band, whereas nitrogen vacancies have the lowest formation energy for the p-type condition, i.e., when Fermi level is near the valance band [26, 53]. Cation vacancies and complexes can have triple, double and single negative charge states. The triply charged states are favorable for higher Al content AlGaN alloys and AlN. Presence of the compensating defects reduces the free carriers despite doping. For example, each triply charged cation vacancy captures three electrons. In the case of p-type conductivity, triple positive charge state is favorable. Experimentally identifying these compensating defects is important to control them and optimize the growth conditions to suppress them. Use of proper characterization tool is also important in such experiments. Al-rich AlGaN alloys can easily become insulator despite Si doping due to insufficient carriers. In such situation electrical characterization methods such as Hall effect measurement is not useful. Photoluminescence (PL) has been a useful tool to detect the presence of impurities and point defects; some of them could act as compensating defects. Using the PL results and the first principles calculations, energy levels of the point defects and corresponding PL emission peaks have been identified in the entire range of AlGaN alloys for both n-doping and p-doping [54, 55]. Intensities of the PL emission peaks can also reveal the crystalline quality of the material. For example, strong band-edge emission compared to the impurity emissions in the PL spectrum indicates high crystalline quality materials, whereas strong impurity transitions compared to the band-edge indicates poor crystalline quality and presence of high density of impurities. Thus, PL results were used as feedback information for optimizing the growth conditions.

Figure 3 shows an example of how PL was utilized for optimizing the growth condition and achieving highly conductive n-type $Al_{0.7}Ga_{0.3}N$ alloy. Dopant solubility in the Al-rich AlGaN alloys was low at normal growth temperature. Growth temperature had to be reduced to increase the solubility of the dopants for heavy doping. A measurable conductivity was achieved in the Al-rich AlGaN epilayers grown on AlN template by Si heavy doping. PL measurement was used as a tool to identify the compensating defects and as feedback information to optimize the growth conditions. As mentioned before, AlN epilayer was first grown on sapphire substrate by MOCVD followed by $Al_{0.7}Ga_{0.3}N$ layer as depicted in the schematic layer structure in Fig. 3a. Heavy doping with Si doping concentration of 3.4×10^{19} cm^{-3} was used. Figure 3b compares the PL spectra of $Al_{0.7}Ga_{0.3}N$ layer samples before and after the optimization of the growth conditions. The PL spectrum of the sample before optimization has a very strong impurity emission peak around 2.91 eV with very weak band edge emission. This indicates the presence of high density of defects and low crystalline quality of the material.

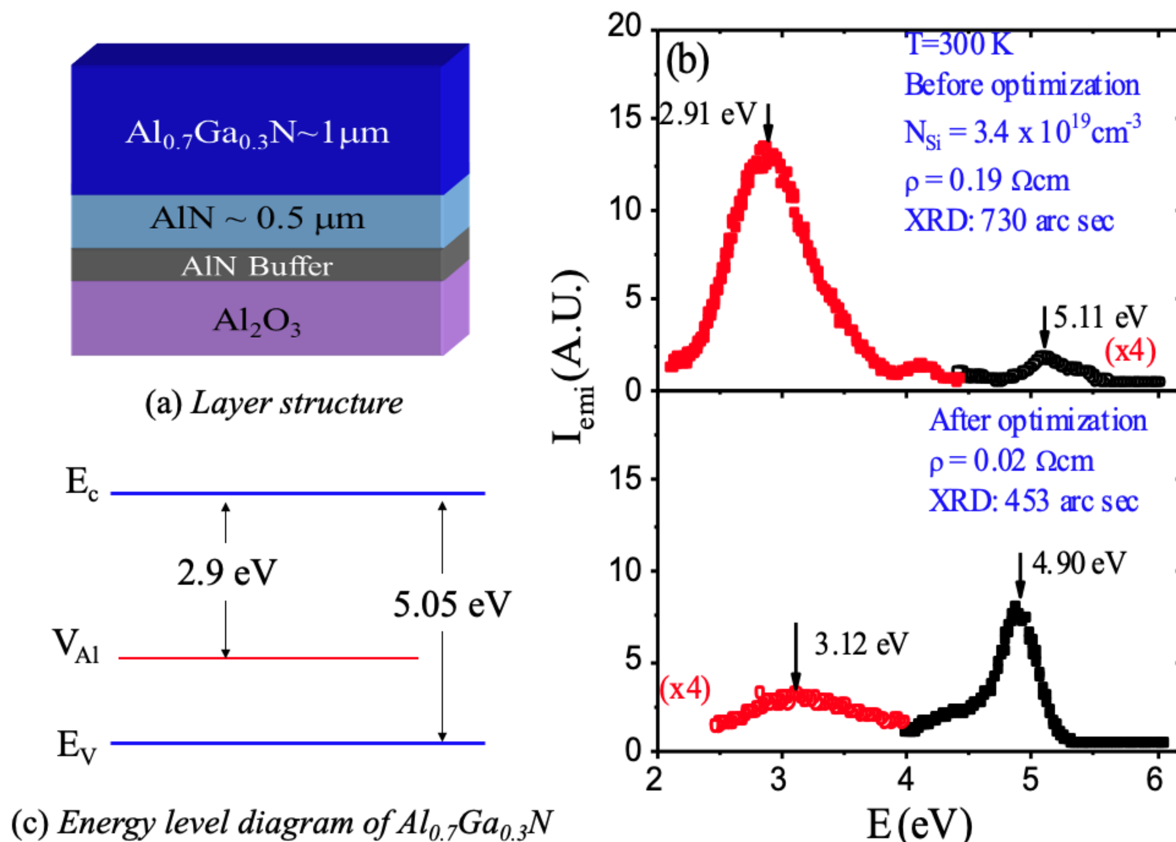

FIGURE 3. a. Layer structure of $Al_{0.7}Ga_{0.3}N$ alloy grown on AlN/sapphire, b. Comparison of PL spectra for optimization of growth conditions in Si-type doming for n-$Al_{0.7}Ga_{0.3}N$ alloy, c. Energy level diagram and corresponding emission lines.

We identified that dominant compensating centers in $Al_{0.7}Ga_{0.3}N$ alloys are triply charged cation vacancies which have energy level about 2.9 eV below conduction band [53, 54]. Fig. 3c shows the energy levels of $Al_{0.7}Ga_{0.3}N$ and corresponding electronic transitions related to the PL emission peaks. During the optimization, the impurity peak was followed by changing the growth conditions. The most effective parameters in the optimization of growth processes were lowering the growth temperature and V/III ratio. After optimization, intensity of the impurity peak and resistivity were decreased almost by one order and the intensity of the band edge $\sim$ 4.9 eV increased by same order. XRD rocking curve results also showed increased crystalline quality of the material which correlates with the PL results. With further optimization of the doping concentration, very high n-type $Al_{0.7}Ga_{0.3}N$ epilayers of resistivity of 0.0075 Ω.cm with free electron concentration of 3.3 x 10^{19} cm^{-3} and mobility of 25 cm^2/Vs at room temperature were obtained [50]. Metallic behavior was obtained with heavy Si-doping and the effective thermal activation energy of Si depends on the doping concentration. It is believed that heavy doping forms an impurity band, and bandgap renormalization occurs due to screening effect. Several other groups also reported achievement of high n-type conductivity in Al-rich AlGaN alloys [27, 56–59]. These results support that Si does not undergo DX transition in AlGaN alloys at least up to x $\sim$ 0.8. N-type conductivity was also observed in the unintentional doped $Al_xGa_{1-x}N$ for x = 0.66 [60]. However, a sharp increase in resistivity was observed for $x > 0.8$ which is not well understood yet. Carbon impurity in Al-rich AlGaN could also be playing role in the electrical compensation in addition to cation vacancies [61]. It is now well understood that material with low dislocation density is essential. Heavy doping can reduce the activation energy. Controlling compensating defects and other impurities is important to enhance the carrier concentration and improve the structural and optical quality of the material.

P- type conductivity of Al-rich AlGaN alloys

The p-type conductivity in AlGaN alloys is not comparable to the n-type one due to the fact that activation energy of the acceptor is large. Historically if one (n- or p-)

type of conductivity is easily achieved, it is challenging to make another type of conductivity in the wide bandgap compound semiconductors. Magnesium (Mg) is a widely used p-type dopant in nitride. Divalent element (magnesium) occupying trivalent cations (Al or Ga) could generate holes. Beryllium is an alternate dopant investigated for p-type doping. As-grown GaN is normally intrinsic n-type. As grown Mg-doped GaN does not show p-type conductivity. Akasaki et al., discovered that low energy electron beam irradiation (LEEBI) activates the Mg acceptors in Mg-doped GaN making the material p-type [7]. In 1992, Nakamura achieved much better p-type conduction with a hole concentration of 3 x 10^{17} cm^{-3} by thermal annealing of the Mg-doped GaN [9]. Mg is passivated by hydrogen during the growth of Mg-doped GaN and annealing is required to release the passivating hydrogen to produce free holes [62–64]. This breakthrough in achieving p-type GaN made it possible to develop nitride based bipolar devices such as LEDs and LDs. Activation energy of Mg for GaN is $\sim$ 160 meV which is already high, and it increases with increasing Al content [65, 66]. Based on the PL results of Mg-doped AlN, activation energy of Mg in AlN was estimated to be around 0.51 eV [67]. This makes it very difficult to produce free holes in the Al-rich ALGaN alloys. Another issue with Mg-doping is the decrease in solubility of Mg in AlGaN when the Al content is increased [62]. The techniques learned from the improvement of n-type conductivity of Al-rich AlGaN alloys were also used such as heavy doping and controlling compensating defects by changing V/III ratio during the growth to improve the p-type conductivity. P-type conductivity of $Al_{0.7}Ga_{0.3}N$ grown on AlN/sapphire reported was $\sim 10^5$ Ω cm at room temperature [15]. With careful optimization of Mg-doping level and V/III ratio, improved resistivity of 47 Ω cm was reported in Mg-doped $Al_{0.7}Ga_{0.3}N$ grown on sapphire substrates [68]. Hole mobility in p-type AlGaN alloys is low. Several other innovative growing techniques such as delta doping [69], AlGaN super lattice doping [70–72], and polarization doping [73] have been used to improve the p-type conductivity. Recently, a low resistivity of 1.4 Ω cm was also reported for $Al_{0.68}Ga_{0.32}N$ alloys by very heavy Mg-doping and compositional grading [74]. Conduction via impurity band was observed in this case. Crystalline quality of the materials still might be an issue in the improvement of p-type conductivity of Al-rich AlGaN alloys. Any improvement especially in the p-type conductivity will have direct impact on the improved performance of the deep UV LEDs.

Deep UV LED structure

In a normal LED structure, the active region is sandwiched between n-type and p-type materials. For efficient optical emission, the active region is designed by making AlGaN multiple QW with low bandgap material and barrier with higher bandgap to confine the carriers to increase radiative recombination probability. The Al-content of the QW in the active region depends on the target emission wavelength. For example, Al content should be $\sim$ 50% for the wavelength of 280 nm. Al content in the barrier, and n- and -type layers must be higher in order to make them transparent to the emitted light. Because of the big disparity of p-type and n-type conductivities of Al-rich AlGaN alloys, device structure of deep UV LEDs needs redesigning, especially in the p-region. Currently used typical device structure of a basic deep UV LEDs structure is shown Figure 4. The LED structure is grown on AlN template (AlN/substrate) followed by the growth of a thick n-type Al-rich AlGaN layer, AlGaN quantum well active region, and p-region layers. Multiple quantum wells are used in the active region for efficient optical emission [75]. Graded Al composition for different shaped quantum well and barriers are also proposed for action region [76]. The p-region is tricky due to the weak p-type conductivity. It has an electron blocking layer, followed by low Al-content p-type AlGaN layer and p-GaN as shown in Fig. 4a. A thick AlN layer on substrate with multiple buffer layers and super lattice layers are also used for strain management and reduction of dislocations. Such layers should not absorb the light emission from active layer.

As the p-type conductivity of AlGaN is not comparable to the n-type conductivity, holes are generated and injected to the active region by using a low Al content p-AlGaN and p-GaN as top layers. Use of p-GaN on the top also make it easy for p-contact. However, these layers absorb the deep UV emitted from the active layer and the light extraction should be done from the bottom layer. So, the substrate must be transparent to the optical emission from the active region. To overcome the disparity due to weak p-type conductivity, several innovative ideas were used on the p-region of the device. One of the crucial layers is the electron blocking layer (EBL). Figure 4b shows the schematic of energy level diagram for a typical deep UV LED structure (layer thickness is not in scale). Because of the much higher conductivity of n-region compared to p-region, electrons can easily overshoot to the p-region. The EBL stops the overflow of electrons into the p-region and confines them in the active layer increasing the probability of radiative recombination [77, 78]. The EBL, however, also imposes a hurdle for hole injection and a large turn on voltage should be applied. Thus, its thickness should be thin and optimized for efficient hole injection. Several other techniques have been employed to improve hole injection such as graded composition [79], Mg-delta doped AlGaN barrier layer [80], multi-quantum barrier EBL [81], and polarization-doped hole injection layer [82].

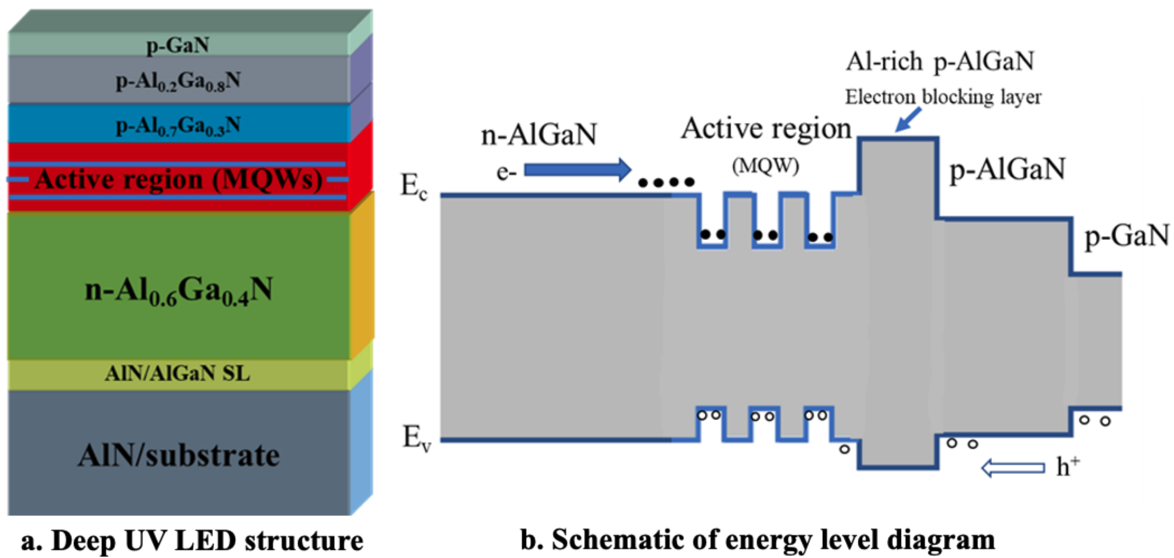

FIGURE 4. a. Layer structure of a typical deep UV LED. b. Schematic of energy level diagram for the deep UV LED structure with major layers.

Challenges and prospects

Despite the demonstrations of deep UV LEDs with emission wavelengths shorter than 300 nm, external efficiency of these LEDs is in the order of 10% or less. Compared to the external efficiency of more than 80% in the blue LEDs, significant improvement is needed. There are many challenges ahead for the development of high power, high efficiency, and long lifetime deep UV LEDs. For better performance of LEDs, four key efficiencies should be improved- radiative efficiency, carrier injection efficiency, electrical efficiency, and light extraction efficiency. In the case of blue LEDs, InGaN quantum wells are used where localization states enhance radiative recombination [83]. This mechanism is not pronounced in deep UV LEDs when AlGaN is used in the active layer. In order to improve the internal quantum efficiency of emission, further improvement of crystalline quality of material is essential. There is a direct correlation of internal efficiency with the threading dislocation density [84]. Enhanced performance of deep UV LEDs was demonstrated with improved crystalline quality by reducing threading dislocations [85–87].

Improvement of p-type conductivity is still a big challenge in AlGaN. A breakthrough in the p-type conductivity of AlGaN is awaited. Finding a new dopant may not be a solution but exploring and investigating nonequilibrium technique could be. In fact, achievement of p-type conductivity in GaN by Mg-doping and subsequent annealing is a nonequilibrium process. Integrated efforts of experimental and theoretical calculation could lead to a solution such as exploring valance band modulation, and co-doping. Due to the large refractive index of AlGaN layers and polarization anisotropic emission from Al-rich AlGaN active layers, light extraction in deep UV LEDs is challenging [41, 88]. Several techniques are used to increase the light extractions including microlens array, reflective photonic crystals (PCs), distributed Bragg reflectors [89–92]. Additional innovative ideas are required in this area. In terms of device fabrication for improved light extraction from the deep UV LEDs, more work is needed in the area of improving the contacts. Developing transparent contacts will also help lower the turn on voltage, enhancing light extraction and thermal management.

There has been significant progress in the material quality of AlN in the last two decades. The progress in the conductivity of the Al-rich AlGaN alloys followed a clear path that reduced dislocation density of materials is the first step before tackling other issues to enhance carrier concentration and mobility. Internal quantum efficiency also significantly increases with decreasing threading dislocations in the material. The dislocation density of AlN grown on sapphire is in the order of 10^9 cm^{-2}. The dislocation density can be reduced by 2-3 orders when later epitaxial overgrowth is used. Recently, impressive progress has been made in the production of wafer size (2 inch) AlN single crystal substrate and available commercially [42–44]. Growth of AlN epilayer and device structure is ideal on the native substrate as the problem due to lattice mismatch and thermal mismatch can be avoided. Average dislocation density of such wafer is around 10^3 cm^{-2}. AlN epilayer with significantly reduced dislocation density can be expected when grown on AlN native sub-

strate. Recently, improved performance with enhanced power and lifetime have been reported for 230 nm deep UV LEDs grown on single crystal AlN substrates [93].

Although dislocation density in the AlN single crystal substrate is very low, most of the substrates available are not transparent to deep UV light. Visually, they look yellowish in color. It could be due to the presence of impurities and point defects such as Al vacancy and vacancy complexes. Additionally, cost will be another issue using single crystal substrate for now. Steady improvements of material quality of AlN wafers reducing defects and impurities are needed. Available wafer size AlN single crystal provides an opportunity to revisit the growth of Al-rich AlGaN materials, doping and device structure by growth on AlN substrate. Recently, Mg-doped AlN was revisited using AlN substrate [94]. A significantly lower Mg-activation energy of Mg in AlN has been reported.

Steady growth of the preformation of deep UV LEDs can be expected based on the recent development in the materials, available of wafer size AlN native substrate and investment in this field due to industrial demands. More opportunities in the design of active regions for improved internal efficiency, efficient hole injection, techniques of improving light extraction efficacy are still available to improve the deep UV LED performance.

ACKNOWLEDGEMENTS

The author would like to acknowledge financial support from ASRC CUNY seed grant and NSF grant (award # 2117286). The author is also grateful to Professors H. X. Jiang and J. Y. Lin currently at Texas Tech University. Special thanks to the Association of Nepali Physicists in America (ANPA) for inviting as a panel speaker in the ANPA Conference 2023.

EDITORS' NOTE

This manuscript was submitted to the Association of Nepali Physicists in America (ANPA) Conference 2023 for publication in the special issue of the Journal of Nepal Physical Society (JNPS).

REFERENCES

1. M. O. Manasreh and I. T. Ferguson, *III-nitride Semiconductor: Growth*, edited by M. O. Manasreh and I. T. Ferguson (Taylor & Francis, 2003).
2. T. Matsuoka, H. Okamoto, M. Nakao, H. Harima, and E. Kurimoto, "Optical bandgap energy of wurtzite inn," Appl. Phys. Lett. **81**, 1246–1248 (2002).
3. J. Wu, W. Walukiewicz, K. M. Yu, J. W. Ager, E. E. Haller, H. Lu, W. J. Schaff, Y. Saito, and Y. Nanishi, "Unusual properties of the fundamental band gap of inn," Appl. Phys. Lett. **80**, 3967–3969 (2002).
4. J. Li, K. B. Nam, M. L. Nakarmi, J. Y. Lin, H. X. Jiang, P. Carrier, and S.-H. Wei, "Band structure and fundamental optical transitions in wurtzite AlN," Appl. Phys. Lett. **83**, 5163–5165 (2003).
5. S. Yoshida, S. Misawa, and S. Gonda, "Improvements on the electrical and luminescent properties of reactive molecular beam epitaxially grown GaN films by using AlN-coated sapphire substrates," Appl. Phys. Lett. **42**, 427–429 (1983).
6. H. Amano, N. Sawaki, I. Akasaki, and Y. Toyoda, "Metalorganic vapor phase epitaxial growth of a high quality gan film using an aln buffer layer," Appl. Phys. Lett. **48**, 353–355 (1986).
7. H. Amano, M. Kito, K. Hiramatsu, and I. Akasaki, "P-type conduction in mg-doped gan treated with low-energy electron beam irradiation (leebi)," Jpn. J. Appl. Phys. **28**, L2112 (1989).
8. S. Nakamura, M. S. M. Senoh, and T. M. T. Mukai, "P-gan/n-ingan/n-gan double-heterostructure blue-light-emitting diodes," Jpn. J. Appl. Phys. **32**, L8 (1993).
9. S. Nakamura, T. Mukai, M. S. M. Senoh, and N. I. N. Iwasa, "Thermal annealing effects on p-type mg-doped gan films," Jpn. J. Appl. Phys. **31**, L139 (1992).
10. S. Nakamura and G. Fassl, *The Blue Laser Diode* (Springer, 1997).
11. Y. Narukawa, M. Ichikawa, D. Sanga, M. Sano, and T. Mukai, "White light emitting diodes with super-high luminous efficacy," J.Phys. D: Appl. Phys. **43**, 354002 (2010).
12. "Compound semiconductor website," `https://compoundsemiconductor.net/article/83304`, accessed: 2022-09-30.
13. J. P. Zhang, A. Chitnis, V. Adivarahan, S. Wu, V. Mandavilli, R. Pachipulusu, M. Shatalov, G. Simin, J. W. Yang, and M. A. Khan, "Milliwatt power deep ultraviolet light-emitting diodes over sapphire with emission at 278 nm," Appl. Phys. Lett. **81**, 4910–4912 (2002).
14. J. Zhang, X. Hu, A. Lunev, J. Deng, Y. Bilenko, T. M. Katona, M. S. Shur, R. Gaska, and M. A. Khan, "AlGaN Deep-Ultraviolet Light-Emitting Diodes," Jpn. J. Appl.Phys. **44**, 7250 (2005).
15. M. L. Nakarmi, K. H. Kim, M. Khizar, Z. Y. Fan, J. Y. Lin, and H. X. Jiang, "Electrical and optical properties of Mg-doped Al0.7Ga0.3N alloys," Appl. Phys. Lett. **86**, 092108 (2005).
16. M. Kneissl, T. Kolbe, C. Chua, V. Kueller, N. Lobo, J. Stellmach, A. Knauer, H. Rodriguez, S. Einfeldt, Z. Yang, N. M. Johnson, and M. Weyers, "Advances in group III-nitride-based deep UV light-emitting diode technology," Semiconductor Science and Technology **26**, 014036 (2011).
17. H. Hirayama, S. Fujikawa, N. Noguchi, J. Norimatsu, T. Takano, K. Tsubaki, and N. Kamata, "222–282 nm AlGaN and InAlGaN-based deep-UV LEDs fabricated on high-quality AlN on sapphire," phys. stat. sol. (a) **206**, 1176–1182 (2009).
18. C. Pernot, M. Kim, S. Fukahori, T. Inazu, T. Fujita, Y. Nagasawa, A. Hirano, M. Ippommatsu, M. Iwaya, S. Kamiyama, I. Akasaki, and H. Amano, "Improved Efficiency of 255–280 nm AlGaN-Based Light-Emitting Diodes," Appl. Phys. Lett. **3**, 061004 (2010).
19. J. R. Grandusky, S. R. Gibb, M. C. Mendrick, C. Moe, M. Wraback, and L. J. Schowalter, "High output power from 260 nm pseudomorphic ultraviolet light-emitting diodes with improved thermal performance," Appl. Phys. Express **4**, 082101 (2011).
20. F. Mehnke, C. Kuhn, M. Guttmann, C. Reich, T. Kolbe, V. Kueller, A. Knauer, M. Lapeyrade, S. Einfeldt, J. Rass, T. Wernicke, M. Weyers, and M. Kneissl, "Efficient charge carrier injection into sub-250 nm AlGaN multiple quantum well light emitting diodes," Appl. Phys. Lett. **105** (2014), 10.1063/1.4892883.
21. S. ichiro Inoue, N. Tamari, and M. Taniguchi, "150 mW deep-ultraviolet light-emitting diodes with large-area AlN nanophotonic light-extraction structure emitting at 265 nm," Appl. Phys. Lett. **110**, 141106 (2017).
22. Y. Taniyasu, M. Kasu, and T. Makimoto, "An aluminium nitride light-emitting diode with a wavelength of 210 nanometres," Nature

441, 325–328 (2006).
23. M. Kneissl and J. Rass, eds., *III-Nitride Ultraviolet Emitters*, Vol. 227 (Springer International Publishing, 2016).
24. A. Janotti and C. G. V. de Walle, "Fundamentals of zinc oxide as a semiconductor," Reports on Progress in Physics **72**, 126501 (2009).
25. J. Li, K. B. Nam, J. Y. Lin, and H. X. Jiang, "Optical and electrical properties of Al-rich AlGaN alloys," Appl. Phys. Lett. **79**, 3245–3247 (2001).
26. C. G. V. de Walle and J. Neugebauer, "First-principles calculations for defects and impurities: Applications to III-nitrides," J. Appl. Phys. **95**, 3851–3879 (2004).
27. Y. Taniyasu, M. Kasu, and N. Kobayashi, "Intentional control of n-type conduction for Si-doped AlN and $Al_xGa_{1-x}N$ ($0.42 \leq x < 1$)," Appl. Phys. Lett. **81**, 1255–1257 (2002).
28. T. Uchida, K. Kusakabe, and K. Ohkawa, "Influence of polymer formation on metalorganic vapor-phase epitaxial growth of AlN," J. Crystal Growth **304**, 133–140 (2007).
29. M. L. Nakarmi, B. Cai, J. Y. Lin, and H. X. Jiang, "Three-step growth method for high quality AlN epilayers," phys. stat. sol. (a) **209**, 126–129 (2012).
30. M. A. Khan, J. N. Kuznia, R. A. Skogman, D. T. Olson, M. M. Millan, and W. J. Choyke, "Low pressure metalorganic chemical vapor deposition of AlN over sapphire substrates," Appl. Phys. Lett. **61**, 2539–2541 (1992).
31. A. Chitnis, J. P. Zhang, V. Adivarahan, M. Shatalov, S. Wu, R. Pachipulusu, V. Mandavilli, and M. A. Khan, "Improved performance of 325-nm emission AlGaN ultraviolet light-emitting diodes," Appl. Phys. Lett. **82**, 2565–2567 (2003).
32. M. Imura, N. Fujimoto, N. Okada, K. Balakrishnan, M. Iwaya, S. Kamiyama, H. Amano, I. Akasaki, T. Noro, T. Takagi, and A. Bandoh, "Annihilation mechanism of threading dislocations in AlN grown by growth form modification method using V/III ratio," J. Crystal Growth **300**, 136–140 (2007).
33. Q. Paduano and D. Weyburne, "Two-step Process for the Metalorganic Chemical Vapor Deposition Growth of High Quality AlN Films on Sapphire," Jpn. J. Appl. Phys. **42**, 1590–1591 (2003).
34. X.-H. Liu, J.-C. Zhang, J. Huang, M.-M. Yang, X.-J. Su, B.-B. Ye, J.-F. Wang, J.-P. Zhang, and K. Xu, "Influence of growth temperature on intrinsic stress distribution in aluminum nitride grown by hydride vapor phase epitaxy," Materials Express **6**, 367–370 (2016).
35. M. Imura, K. Nakano, T. Kitano, N. Fujimoto, G. Narita, N. Okada, K. Balakrishnan, M. Iwaya, S. Kamiyama, H. Amano, I. Akasaki, K. Shimono, T. Noro, T. Takagi, and A. Bandoh, "Microstructure of epitaxial lateral overgrown AlN on trench-patterned AlN template by high-temperature metal-organic vapor phase epitaxy," Appl. Phys. Lett. **89** (2006), 10.1063/1.2364460.
36. J. Li, K. B. Nam, M. L. Nakarmi, J. Y. Lin, and H. X. Jiang, "Band-edge photoluminescence of AlN epilayers," Appl. Phys. Lett. **81**, 3365–3367 (2002).
37. B. N. Pantha, R. Dahal, M. L. Nakarmi, N. Nepal, J. Li, J. Y. Lin, H. X. Jiang, Q. S. Paduano, and D. Weyburne, "Correlation between optoelectronic and structural properties and epilayer thickness of AlN," Appl. Phys. Lett. **90** (2007), 10.1063/1.2747662.
38. J. Han, T.-B. Ng, R. M. Biefeld, M. H. Crawford, and D. M. Follstaedt, "The effect of H2 on morphology evolution during GaN metalorganic chemical vapor deposition," Appl. Phys. Lett. **71**, 3114–3116 (1997).
39. D. G. Zhao, J. J. Zhu, Z. S. Liu, S. M. Zhang, H. Yang, and D. S. Jiang, "Surface morphology of AlN buffer layer and its effect on GaN growthby metalorganic chemical vapor deposition," Appl. Phys. Lett. **85**, 1499–1501 (2004).
40. J. Li, Z. Y. Fan, R. Dahal, M. L. Nakarmi, J. Y. Lin, and H. X. Jiang, "200 nm deep ultraviolet photodetectors based on AlN," Appl. Phys. Lett. **89** (2006), 10.1063/1.2397021.
41. K. B. Nam, J. Li, M. L. Nakarmi, J. Y. Lin, and H. X. Jiang, "Unique optical properties of AlGaN alloys and related ultraviolet emitters," Appl. Phys. Lett. **84**, 5264–5266 (2004).
42. R. T. Bondokov, S. G. Mueller, K. E. Morgan, G. A. Slack, S. Schujman, M. C. Wood, J. A. Smart, and L. J. Schowalter, "Large-area AlN substrates for electronic applications: An industrial perspective," J. Crystal Growth **310**, 4020–4026 (2008).
43. R. Dalmau, B. Moody, J. Xie, R. Collazo, and Z. Sitar, "Characterization of dislocation arrays in AlN single crystals grown by PVT," physica status solidi (a) **208**, 1545–1547 (2011).
44. C. Hartmann, A. Dittmar, J. Wollweber, and M. Bickermann, "Bulk AlN growth by physical vapour transport," Semiconductor Science and Technology **29**, 084002 (2014).
45. J. Neugebauer and C. G. Van de Walle, "Atomic geometry and electronic structure of native defects in GaN," Phys. Rev. B **50**, 8067–8070 (1994).
46. T. Mattila and R. M. Nieminen, "Ab initio study of oxygen point defects in GaAs, GaN, and AlN," Phys. Rev. B **54**, 16676–16682 (1996).
47. A. J. Ptak, L. J. Holbert, L. Ting, C. H. Swartz, M. Moldovan, N. C. Giles, T. H. Myers, P. V. Lierde, C. Tian, R. A. Hockett, S. Mitha, A. E. Wickenden, D. D. Koleske, and R. L. Henry, "Controlled oxygen doping of GaN using plasma assisted molecular-beam epitaxy," Appl. Phys. Lett. **79**, 2740–2742 (2001).
48. M. D. McCluskey, N. M. Johnson, C. G. V. de Walle, D. P. Bour, M. Kneissl, and W. Walukiewicz, "Metastability of Oxygen Donors in AlGaN," Phys. Rev. Lett. **80**, 4008–4011 (1998).
49. W. Götz, N. M. Johnson, C. Chen, H. Liu, C. Kuo, and W. Imler, "Activation energies of Si donors in GaN," Appl. Phys. Lett. **68**, 3144–3146 (1996).
50. M. L. Nakarmi, K. H. Kim, K. Zhu, J. Y. Lin, and H. X. Jiang, "Transport properties of highly conductive n-type al-rich $Al_xGa_{1-x}N(x \geq 0.7)$," Appl. Phys. Lett. **85**, 3769–3771 (2004).
51. C. Wetzel, T. Suski, J. W. A. III, E. R. Weber, E. E. Haller, S. Fischer, B. K. Meyer, R. J. Molnar, and P. Perlin, "Pressure Induced Deep Gap State of Oxygen in GaN," Phys. Rev. Lett. **78**, 3923–3926 (1997).
52. C. Skierbiszewski, T. Suski, M. Leszczynski, M. Shin, M. Skowronski, M. D. Bremser, and R. F. Davis, "Evidence for localized Si-donor state and its metastable properties in AlGaN," Appl. Phys. Lett. **74**, 3833–3835 (1999).
53. C. Stampfl and C. G. V. de Walle, "Doping of $Al_xGa_{1-x}N$," Appl. Phys. Lett. **72**, 459–461 (1998).
54. K. B. Nam, M. L. Nakarmi, J. Y. Lin, and H. X. Jiang, "Deep impurity transitions involving cation vacancies and complexes in AlGaN alloys," Appl. Phys. Lett. **86** (2005), 10.1063/1.1943489.
55. M. L. Nakarmi, N. Nepal, J. Y. Lin, and H. X. Jiang, "Photoluminescence studies of impurity transitions in Mg-doped AlGaN alloys," Appl. Phys. Lett. **94** (2009), 10.1063/1.3094754.
56. A. S. Almogbel, C. J. Zollner, B. K. Saifaddin, M. Iza, J. Wang, Y. Yao, M. Wang, H. Foronda, I. Prozheev, F. Tuomisto, A. Albadri, S. Nakamura, S. P. DenBaars, and J. S. Speck, "Growth of highly conductive Al-rich AlGaN:Si with low group-III vacancy concentration," AIP Advances **11** (2021), 10.1063/5.0066652.
57. F. Mehnke, T. Wernicke, H. Pingel, C. Kuhn, C. Reich, V. Kueller, A. Knauer, M. Lapeyrade, M. Weyers, and M. Kneissl, "Highly conductive n-$Al_xGa_{1-x}N$ layers with aluminum mole fractions above 80%," Appl. Phys. Lett. **103**, 212109 (2013).
58. P. Cantu, S. Keller, U. K. Mishra, and S. P. DenBaars, "Metalorganic chemical vapor deposition of highly conductive Al0.65Ga0.35N films," Appl. Phys. Lett. **82**, 3683–3685 (2003).
59. Y. Nishikawa, K. Ueno, A. Kobayashi, and H. Fujioka, "Preparation of degenerate n-type $Al_xGa_{1-x}N$ ($0 \leq x \leq 0.81$) with record low resistivity by pulsed sputtering deposition," Appl. Phys. Lett. **122**, 232102 (2023).
60. M. L. Nakarmi, N. Nepal, J. Y. Lin, and H. X. Jiang, "Unintentionally doped n-type Al0.67Ga0.33N epilayers," Appl. Phys. Lett. **86** (2005), 10.1063/1.1954875.
61. I. Prozheev, F. Mehnke, T. Wernicke, M. Kneissl, and F. Tuomisto, "Electrical compensation and cation vacancies in Al rich Si-doped

AlGaN," Appl. Phys. Lett. **117** (2020), 10.1063/5.0016494.

62. J. Neugebauer and C. G. V. de Walle, "Role of hydrogen in doping of GaN," Appl. Phys. Lett. **68**, 1829–1831 (1996).
63. W. Götz, N. M. Johnson, J. Walker, D. P. Bour, H. Amano, and I. Akasaki, "Hydrogen passivation of Mg acceptors in GaN grown by metalorganic chemical vapor deposition," Appl. Phys. Lett. **67**, 2666–2668 (1995).
64. Y. Okamoto, M. Saito, and A. Oshiyama, "First-Principles Calculations on Mg Impurity and Mg–H Complex in GaN," Jpn. J. Appl. Phys. **35**, L807 (1996).
65. J. Li, T. N. Oder, M. L. Nakarmi, J. Y. Lin, and H. X. Jiang, "Optical and electrical properties of Mg-doped p-type $al_x ga_{1-x} n$," Appl. Phys. Lett. **80**, 1210–1212 (2002).
66. T. Tanaka, A. Watanabe, H. Amano, Y. Kobayashi, I. Akasaki, S. Yamazaki, and M. Koike, "p-type conduction in Mg-doped GaN and $Al_{0.08}Ga_{0.92}N$ grown by metalorganic vapor phase epitaxy," Appl. Phys. Lett. **65**, 593–594 (1994).
67. K. B. Nam, M. L. Nakarmi, J. Li, J. Y. Lin, and H. X. Jiang, "Mg acceptor level in AlN probed by deep ultraviolet photoluminescence," Appl. Phys. Lett. **83**, 878–880 (2003).
68. T. Kinoshita, T. Obata, H. Yanagi, and S. ichiro Inoue, "High p-type conduction in high-Al content Mg-doped AlGaN," Appl. Phys. Lett. **102** (2013), 10.1063/1.4773594.
69. M. L. Nakarmi, K. H. Kim, J. Li, J. Y. Lin, and H. X. Jiang, "Enhanced p-type conduction in GaN and AlGaN by Mg-δ-doping," Appl. Phys. Lett. **82**, 3041–3043 (2003).
70. A. Allerman, M. Crawford, M. Miller, and S. Lee, "Growth and characterization of Mg-doped AlGaN–AlN short-period superlattices for deep-UV optoelectronic devices," J. Crystal Growth **312**, 756–761 (2010).
71. T. C. Zheng, W. Lin, R. Liu, D. J. Cai, J. C. Li, S. P. Li, and J. Y. Kang, "Improved p-type conductivity in Al-rich AlGaN using multidimensional Mg-doped superlattices," Scientific Reports **6**, 21897 (2016).
72. K. Ebata, J. Nishinaka, Y. Taniyasu, and K. Kumakura, "High hole concentration in Mg-doped AlN/AlGaN superlattices with high Al content," Jpn. J. Appl. Phys. **57**, 04FH09 (2018).
73. J. Simon, V. Protasenko, C. Lian, H. Xing, and D. Jena, "Polarization-Induced Hole Doping in Wide–Band-Gap Uniaxial Semiconductor Heterostructures," Science **327**, 60–64 (2010).
74. S. Rathkanthiwar, P. Reddy, B. Moody, C. Quiñones-García, P. Bagheri, D. Khachariya, R. Dalmau, S. Mita, R. Kirste, R. Collazo, and Z. Sitar, "High p-conductivity in AlGaN enabled by polarization field engineering," Appl. Phys. Lett. **122** (2023), 10.1063/5.0143427.
75. H. Hirayama, Y. Enomoto, A. Kinoshita, A. Hirata, and Y. Aoyagi, "Efficient 230–280 nm emission from high-Al-content AlGaN-based multiquantum wells," Appl. Phys. Lett. **80**, 37–39 (2002).
76. I. Mazumder, K. Sapra, H. Aagiwal, A. Chauhan, M. Mathew, and K. Singh, "Effect of graded Al composition in w-shaped quantum wells and Δ-shaped quantum barriers on performance of AlGaN based UV-C light emitting diodes," Materials Science and Engineering: B **296**, 116624 (2023).
77. F. Mehnke, C. Kuhn, M. Guttmann, C. Reich, T. Kolbe, V. Kueller, A. Knauer, M. Lapeyrade, S. Einfeldt, J. Rass, T. Wernicke, M. Weyers, and M. Kneissl, "Efficient charge carrier injection into sub 250 nm AlGaN multiple quantum well light emitting diodes," Appl. Phys. Lett. **105**, 051113 (2014).
78. J.-Y. Chang, M.-F. Huang, F.-M. Chen, B.-T. Liou, Y.-H. Shih, and Y.-K. Kuo, "Effects of quantum barriers and electron-blocking layer in deep-ultraviolet light-emitting diodes," J. Phys. D: Applied Physics **51**, 075106 (2018).
79. J. Yan, J. Wang, P. Cong, L. Sun, N. Liu, Z. Liu, C. Zhao, and J. Li, "Improved performance of UV-LED by p-AlGaN with graded composition," phys. stat. sol. c **8**, 461–463 (2011).
80. T.-Y. Wang, W.-C. Lai, S.-Y. Sie, S.-P. Chang, Y.-R. Wu, Y.-Z. Chiou, C.-H. Kuo, and J.-K. Sheu, "AlGaN-based deep ultraviolet light emitting diodes with magnesium delta-doped AlGaN last barrier," Appl. Phys. Lett. **117** (2020), 10.1063/5.0026911.
81. H. Hirayama, Y. Tsukada, T. Maeda, and N. Kamata, "Marked Enhancement in the Efficiency of Deep-Ultraviolet AlGaN Light-Emitting Diodes by Using a Multiquantum-Barrier Electron Blocking Layer," Appl. Phys. Express **3**, 031002 (2010).
82. T. Kolbe, A. Knauer, J. Rass, H. K. Cho, S. Hagedorn, F. Bilchenko, A. Muhin, J. Ruschel, M. Kneissl, S. Einfeldt, and M. Weyers, "234 nm far-ultraviolet-C light-emitting diodes with polarization-doped hole injection layer," Appl. Phys. Lett. **122** (2023), 10.1063/5.0143661.
83. S. Chichibu, T. Azuhata, T. Sota, and S. Nakamura, "Luminescences from localized states in InGaN epilayers," Appl. Phys. Lett. **70**, 2822–2824 (1997).
84. K. Ban, J. ichi Yamamoto, K. Takeda, K. Ide, M. Iwaya, T. Takeuchi, S. Kamiyama, I. Akasaki, and H. Amano, "Internal Quantum Efficiency of Whole-Composition-Range AlGaN Multiquantum Wells," Appl. Phys. Express **4**, 052101 (2011).
85. H. Hirayama, T. Yatabe, N. Noguchi, T. Ohashi, and N. Kamata, "231–261nm AlGaN deep-ultraviolet light-emitting diodes fabricated on AlN multilayer buffers grown by ammonia pulse-flow method on sapphire," Appl. Phys. Lett. **91**, 071901 (2007).
86. J. Ruschel, J. Glaab, N. Susilo, S. Hagedorn, S. Walde, E. Ziffer, H. K. Cho, N. L. Ploch, T. Wernicke, M. Weyers, S. Einfeldt, and M. Kneissl, "Reliability of UVC LEDs fabricated on AlN/sapphire templates with different threading dislocation densities," Appl. Phys. Lett. **117** (2020), 10.1063/5.0027769.
87. N. Lobo-Ploch, F. Mehnke, L. Sulmoni, H. K. Cho, M. Guttmann, J. Glaab, K. Hilbrich, T. Wernicke, S. Einfeldt, and M. Kneissl, "Milliwatt power 233 nm AlGaN-based deep UV-LEDs on sapphire substrates," Appl. Phys. Lett. **117** (2020), 10.1063/5.0015263.
88. C. Reich, M. Guttmann, M. Feneberg, T. Wernicke, F. Mehnke, C. Kuhn, J. Rass, M. Lapeyrade, S. Einfeldt, A. Knauer, V. Kueller, M. Weyers, R. Goldhahn, and M. Kneissl, "Strongly transverse-electric-polarized emission from deep ultraviolet AlGaN quantum well light emitting diodes," Appl. Phys. Lett. **107** (2015), 10.1063/1.4932651.
89. M. Khizar, Z. Y. Fan, K. H. Kim, J. Y. Lin, and H. X. Jiang, "Nitride deep-ultraviolet light-emitting diodes with microlens array," Appl. Phys. Lett. **86** (2005), 10.1063/1.1914960.
90. J. Rass, H. K. Cho, M. Guttmann, D. Prasai, J. Ruschel, T. Kolbe, and S. Einfeldt, "Enhanced light extraction efficiency of far-ultraviolet-C LEDs by micro-LED array design," Appl. Phys. Lett. **122** (2023), 10.1063/5.0154031.
91. Y. Kashima, N. Maeda, E. Matsuura, M. Jo, T. Iwai, T. Morita, M. Kokubo, T. Tashiro, R. Kamimura, Y. Osada, H. Takagi, and H. Hirayama, "High external quantum efficiency (10%) AlGaN-based deep-ultraviolet light-emitting diodes achieved by using highly reflective photonic crystal on p-AlGaN contact layer," Appl. Phys. Express **11**, 012101 (2018).
92. T. Nakashima, K. Takeda, H. Shinzato, M. Iwaya, S. Kamiyama, T. Takeuchi, I. Akasaki, and H. Amano, "Combination of Indium–Tin Oxide and SiO2 /AlN Dielectric Multilayer Reflective Electrodes for Ultraviolet-Light-Emitting Diodes," Jpn. J. Appl. Phys. **52**, 08JG07 (2013).
93. H. Kobayashi, K. Sato, Y. Okuaki, T. Lee, T. Morishita, H. Goto, and N. Kuze, "Milliwatt-power sub-230-nm algan leds with > 1500 h lifetime on a single-crystal aln substrate with many quantum wells for effective carrier injection," Appl. Phys. Lett. **122** (2023), 10.1063/5.0139970.
94. R. Ishii, A. Yoshikawa, M. Funato, and Y. Kawakami, "Revisiting the substitutional Mg acceptor binding energy of AlN," Phys. Rev. B **108**, 035205 (2023).